

# Magnetoelasticity in $\text{ACr}_2\text{O}_4$ spinel oxides

V. Kocsis,<sup>1</sup> S. Bordács,<sup>1,2</sup> D. Varjas,<sup>1</sup> K. Penc,<sup>3</sup> A. Abouelsayed,<sup>4</sup>  
C. A. Kuntscher,<sup>4</sup> K. Ohgushi,<sup>5</sup> Y. Tokura,<sup>2,6,7</sup> and I. Kézsmárki<sup>1</sup>

<sup>1</sup>*Department of Physics, Budapest University of Technology and Economics and Condensed Matter Research Group of the Hungarian Academy of Sciences, 1111 Budapest, Hungary*

<sup>2</sup>*Quantum-Phase Electronics Center, Department of Applied Physics, University of Tokyo, Tokyo 113-8656, Japan*

<sup>3</sup>*Institute for Solid State Physics and Optics, Wigner Research Centre for Physics, Hungarian Academy of Sciences, H-1525 Budapest, Hungary*

<sup>4</sup>*Experimentalphysik 2, Universität Augsburg, D-86135 Augsburg, Germany*

<sup>5</sup>*Institute for Solid State Physics, University of Tokyo, Kashiwa, Chiba 277-8581, Japan*

<sup>6</sup>*Department of Applied Physics, University of Tokyo, Tokyo 113-8656, Japan*

<sup>7</sup>*Cross-correlated Materials Group (CMRG) and Correlated Electron Research Group (CERG), RIKEN Advanced Science Institute, Wako 351-0198, Japan*

Dynamical properties of the lattice structure was studied by optical spectroscopy in  $\text{ACr}_2\text{O}_4$  chromium spinel oxide magnetic semiconductors over a broad temperature region of  $T=10\text{--}335\text{ K}$ . The systematic change of the A-site ions ( $A=\text{Mn, Fe, Co, Ni}$  and  $\text{Cu}$ ) showed that the occupancy of 3d orbitals on the A-site, has strong impact on the lattice dynamics. For compounds with orbital degeneracy ( $\text{FeCr}_2\text{O}_4$ ,  $\text{NiCr}_2\text{O}_4$  and  $\text{CuCr}_2\text{O}_4$ ), clear splitting of infrared-active phonon modes and/or activation of silent vibrational modes have been observed upon the Jahn-Teller transition and at the onset of the subsequent long-range magnetic order. Although  $\text{MnCr}_2\text{O}_4$  and  $\text{CoCr}_2\text{O}_4$  show multiferroic and magnetoelectric character, no considerable magnetoelasticity was found in spinel compounds without orbital degeneracy as they closely preserve the high-temperature cubic spinel structure even in their magnetic ground state. Besides lattice vibrations, intra-atomic 3d-3d transitions of the  $A^{2+}$  ions were also investigated to determine the crystal field and Racah parameters and the strength of the spin-orbit coupling.

PACS numbers:

## Introduction

Effect of spin ordering on the symmetry and lattice parameters of magnetic crystals, termed as magnetoelasticity, has recently attracted remarkable interest in multiferroic materials and complex magnets. This is because magnetoelasticity is closely related to the magnetocapacitance and other magnetoelectric phenomena [1–3]. The dynamical coupling between lattice vibrations and spin-wave excitations plays also a crucial role in the electromagnon excitations of manganese oxides [4–6]. For several chromium spinel oxides, the materials in the focus of the present study, multiferroic ordering has been reported at low temperatures and strong magnetic field induced changes were also found in their dielectric response [1, 7–10]. In order to reveal the nature and origin of spin-phonon coupling governing magneto-elasticity, optical probe of lattice vibrations has been shown to be an efficient tool for a broad class of chromium spinel oxides and chalcogenides with non-magnetic A-site ions [11–14].

At high temperatures  $\text{ACr}_2\text{O}_4$  chromium spinel oxides have the normal cubic spinel structure corresponding to the space group of  $\text{Fd}\bar{3}\text{m}$  as shown in Fig. 1(a). Within this structure  $A^{2+}$  ions form a diamond lattice with tetrahedral oxygen environment, while magnetic  $\text{Cr}^{3+}$  ions surrounded by octahedral oxygen cages form a pyrochlore sublattice. In the local crystal field of oxygen ions, the 3d orbitals of a  $\text{Cr}^{3+}$  ion are split into a low-lying  $t_{2g}$  triplet

and a higher-energy  $e_g$  doublet, while the orbitals of an  $A^{2+}$  ion are split into a lower  $e$  doublet and a higher  $t_2$  triplet as illustrated in Fig. 1(b). The presence of magnetic moment and orbital degeneracy on the A-site ions can change the magnetic and structural properties in chromium spinel oxides in two ways as compared to those members of the  $\text{ACr}_2\text{O}_4$  family where  $\text{Cr}^{3+}$  is the only magnetic ion.

First, the antiferromagnetic  $J_{Cr-Cr}$  exchange interaction between neighboring  $\text{Cr}^{3+}$  ions leads to a highly frustrated ground state on the pyrochlore sublattice. This frustration can only be released by the so-called spin-Jahn-Teller effect for compounds with nonmagnetic A-site ions, where lattice distortions induce differences between the exchange coefficients originally uniform for each  $\text{Cr}^{3+}\text{--Cr}^{3+}$  pairs. This removes the spin degeneracy of the ground state and consequently long-range magnetic order can develop as was observed at low temperatures in case of  $\text{ZnCr}_2\text{O}_4$  [11, 12] and  $\text{CdCr}_2\text{O}_4$  [13]. In contrast, if A-site ions are magnetic, the coupling of  $S=3/2$   $\text{Cr}^{3+}$  spins to the A-site spins on the bipartite diamond lattice removes the magnetic frustration and the magnetic ordering occurs at much higher temperatures comparable to the energy scale of the exchange interactions.

Second, if A-site ions have orbital degeneracy in the cubic spinel structure, it is lifted by a cooperative Jahn-Teller distortion resulting to a tetragonal structure with

space group  $I4_1/amd$  already in the high-temperature paramagnetic phase [15–18] and the onset of magnetic order may result in further reduction of the lattice symmetry through a spin-lattice coupling. On the other hand, chromium oxide spinels with magnetic A sites but without orbital degeneracy are reported to nearly maintain the cubic structure even in their low-temperature magnetic state [7, 19, 20]. Besides spinel chromites, the impact of orbital degeneracy on the magnetic and structural properties is clearly manifested in vanadium oxide spinels, where both diamond and pyrochlore sublattices can host orbital degeneracy. The most peculiar example is  $FeV_2O_4$  [21], which exhibits successive structural transitions due to the interplay between the Jahn-Teller effect on the two sublattices and the influence of the spin order.

In the present paper we perform a systematic optical study of  $ACr_2O_4$  chromium spinels having magnetic ions also on the A site ( $A=Mn, Fe, Co, Ni$  and  $Cu$ ). In sequence of increasing number of 3d electrons on the A-site ions,  $A=Fe, Ni$  and  $Cu$  compounds are Jahn-Teller active ions, that is they show orbital degeneracy, while  $MnCr_2O_4$  and  $CoCr_2O_4$  spinels have no orbital degrees of freedom (see Fig. 1(b)). Our main purpose is to reveal the key parameters responsible for the lowering of the lattice symmetry associated with their magnetic ordering, i.e. the origin of magnetoelasticity in these compounds, by an infrared optical study of their lattice dynamics. We also investigate the intra-atomic  $3d-3d$  transitions of the A-site ions to reveal their electronic state of these magnetic ions.

Kaplan and Menyuk [22] proposed that for  $J_{A-Cr}$  (exchange coupling between spins of neighboring  $A^{2+}$  and  $Cr^{3+}$  ions) sufficiently strong relative to  $J_{Cr-Cr}$ , the magnetic ground state becomes unique and non-collinear magnetic orders with three different magnetic sublattices can develop. This has been verified experimentally for all these compounds.  $CoCr_2O_4$  exhibits ferrimagnetic order below  $T_C=93$  K and an incommensurate conical spin-order develops under  $T_S=27$  K, which becomes commensurate to the lattice at  $T_{lock-in}=13$  K [7, 23–26]. In the conical magnetic phase the presence of spontaneous electric polarization and ferrotoroidicity were reported [7]. In  $MnCr_2O_4$  the ferrimagnetic transition occurs at  $T_C=48$  K, while the onset of the long-range conical order takes place at  $T_S=14$  K [19, 25, 26]. Similarly,  $FeCr_2O_4$  becomes a ferrimagnet below  $T_C=93$  K and the conical order sets in at  $T_S=35$  K [26–29]. Ferroelectric polarization was observed in this material below  $T_C$  [10]. The magnetic structures of  $NiCr_2O_4$  and  $CuCr_2O_4$  are rather different from the former compounds. According to magnetization measurements  $NiCr_2O_4$  becomes a collinear ferrimagnet at  $T_C=74$  K, where the simultaneous lowering of the lattice symmetry to orthorhombic was verified by X-ray scattering measurements [30]. Below  $T_S=31$  K this compound exhibits a Yafet-Kittel-type

canted ferrimagnetic order [31]. In  $CuCr_2O_4$  the Yafet-Kittel-type magnetic order emerges right from the paramagnetic state at  $T_C=152$  K [26, 32].

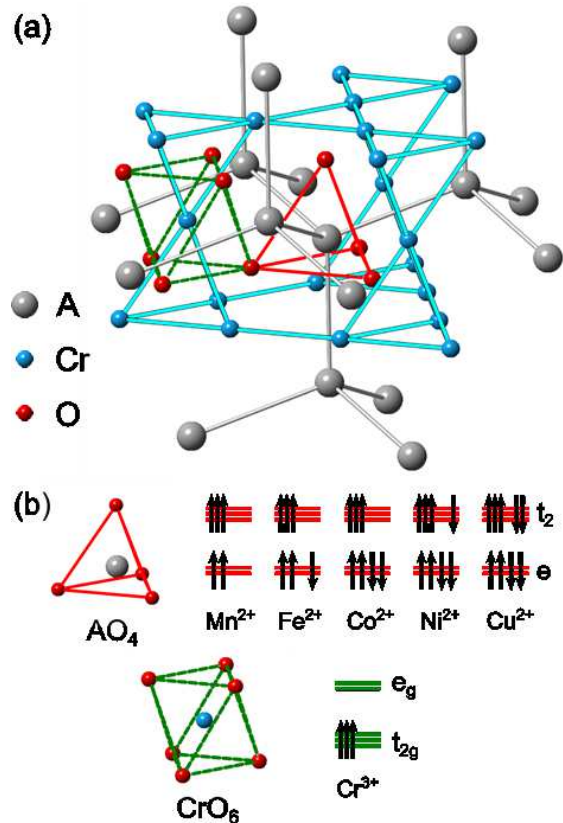


FIG. 1: (a) In the structure of  $ACr_2O_4$  spinels the  $Cr^{3+}$  ions (light blue spheres) and the  $A^{2+}$  ions (grey spheres) are located on a pyrochlore and a diamond lattice, respectively. The oxygens (red spheres) form octahedral environment around  $Cr^{3+}$  ions, while  $A^{2+}$  ions are surrounded by tetrahedral oxygen cages. (b) Electron configuration of  $Cr^{3+}$  ion and A-site ions with increasing electron number on the 3d shell. Here, the splitting due to the local crystal field of the ions in the cubic phase and the effect of Hund coupling are only taken into account.

### Experimental techniques and data analysis

Single crystals of  $ACr_2O_4$  for  $A=Mn, Fe, Co$  with typical linear dimensions of  $300-600 \mu m$  were synthesized by chemical vapour transport, while  $CuCr_2O_4$  was made by flux deposition method as described elsewhere [26]. We adopted flux deposition method of B. M. Wanklyn et al. [33] using solely  $PbO$  flux in order to grow  $NiCr_2O_4$ .

Unpolarized normal incidence reflectivity spectra were studied on the (111) surface for  $A=Mn, Fe, Co, Ni$  and on the (010) surface of  $CuCr_2O_4$  over the temperature range of  $T=10-335$  K with a Bruker IFS 66v/s Fourier-transform IR spectrometer coupled to a micro-scope (Bruker Hyperion). The lattice vibrations were

found to be sensitive to polishing induced mechanical strain, thus, reflectivity spectra were measured on as-grown surfaces at low energies,  $\omega=100\text{-}7700\text{ cm}^{-1}$ . The surface roughness of  $\text{MnCr}_2\text{O}_4$  and  $\text{NiCr}_2\text{O}_4$  samples demanded to use of polished surfaces in order to avoid light scattering at higher energies. Correspondingly, reflectivity spectra were also recorded over  $\omega=1700\text{-}24000\text{ cm}^{-1}$  on polished surfaces. Reflectivity spectrum of each compound was measured up to  $\omega=250000\text{ cm}^{-1}$  at room temperature [26, 34].

Optical conductivity spectra were obtained from the reflectivity data by Kramers-Kronig transformation. The low-energy part of the measured reflectivity spectra was extrapolated to zero photon energy as a constant value, while the high-energy part was assumed to follow the free electron model above  $\omega=1000000\text{ cm}^{-1}$ . The advantage of the optical conductivity spectra versus the reflectivity spectra is that phonon excitations appear as sharp peaks in the former, while close resonances are more difficult to resolve in the reflectivity data. In the analysis of the optical phonon modes we fitted the corresponding low-energy part of the optical conductivity spectra with a sum of Lorentzian peaks according to

$$\sigma(\omega) = -i\omega\epsilon_o \left( \epsilon_\infty - 1 + \sum_{i=1} \frac{S_i}{\omega_i^2 - \omega^2 - i\gamma_i\omega} \right), \quad (1)$$

where  $S_i$ ,  $\omega_i$  and  $\gamma_i$  stand for the oscillator strength, the resonance frequency and the damping rate of the modes,  $\epsilon_o$  is the vacuum permittivity and  $\epsilon_\infty$  is the dielectric constant at high energies.

## Results

The measured reflectivity and the corresponding optical conductivity spectra are plotted over common energy scales for  $\text{ACr}_2\text{O}_4$  spinels (A=Mn, Fe, Co, Ni and Cu) in Fig. 2 at T=10 K. At the high-energy side the upturn of the optical conductivity corresponds to a band gap of  $\Delta \approx 2.5\text{ eV}$  characteristic to these chromium spinel oxides. The gap value is not significantly influenced by the variation of the A-site ions, therefore, the lowest-energy interband transition is mainly related to the O 2p  $\rightarrow$  Cr 3d charge transfer excitations. Below the optical gap weak excitations exist in the visible and near infrared region. Since these structures are sensitive to the change of the A-site ion they are assigned as intra-atomic  $3d\text{-}3d$  transitions of the tetrahedrally coordinated A cations in agreement with former optical studies [26]. A broad and low-intensity hump at E=1.6 eV is the only structure common in each spectra. This feature is due to the  $3d\text{-}3d$  transitions of the  $\text{Cr}^{3+}$  ions. Finally, in the low-energy range ( $\omega=100\text{-}700\text{ cm}^{-1}$ ) optical phonon excitations characteristic to the lattice structure are present. In the following sections dependence of the phonon ex-

citations and the  $3d\text{-}3d$  transitions on the A-site cations and the temperature are studied.

### Lattice vibrations in $\text{ACr}_2\text{O}_4$ spinels without orbital degree of freedom

According to powder X-ray diffraction measurements the lattice symmetry for A=Mn, Fe, Co corresponds to the cubic space group  $Fd\bar{3}m$  at room temperature, while in the case of A=Ni, Cu the symmetry is already tetragonal with the space group  $I4_1/amd$  [17, 26].

The factor group analysis for cubic spinels ( $Fd\bar{3}m$  space group,  $m\bar{3}m$  ( $O_h$ ) point group) yields 16 optical phonon modes in the  $\Gamma$  point:

$$\begin{aligned} \Gamma(\text{ACr}_2\text{O}_4)_{Fd\bar{3}m} = & A_{1g}(\text{R}) \oplus 2A_{2u}(\text{S}) \oplus E_g(\text{R}) \oplus \\ & \oplus 2E_u(\text{S}) \oplus T_{1g}(\text{S}) \oplus 4T_{1u}(\text{IR}) \oplus \\ & \oplus 3T_{2g}(\text{R}) \oplus 2T_{2u}(\text{S}), \end{aligned} \quad (2)$$

where abbreviations IR, R and S refer to infrared-active, Raman-active and silent modes, respectively. Thus, in the cubic phase four  $T_{1u}(\text{IR})$  modes are expected to appear in the optical spectra, all of which have three-fold degeneracy. When the lattice symmetry is reduced to tetragonal each of these  $T_{1u}$  lattice vibrations are split into an  $A_{2u}(\text{IR})$  singlet and an  $E_u(\text{IR})$  doublet mode. Furthermore, the two originally silent  $T_{2u}$  phonon modes can split into an infrared-active  $E_u(\text{IR})$  doublet and a silent  $B_{2u}$  singlet. If the symmetry of the lattice further lowered the degeneracy of each mode is completely lifted.

Optical conductivity spectra of  $\text{MnCr}_2\text{O}_4$  and  $\text{CoCr}_2\text{O}_4$ , spinels with no orbital degrees of freedom, are shown in Fig. 3 and Fig. 4, respectively. All four infrared active  $T_{1u}(\text{IR})$  optical phonon modes expected in the cubic phase are observed at room temperature for both compounds. As the temperature is decreased to T=10 K the lifetime of each phonon mode is increased by  $\sim 30\%$ . The detailed temperature dependence of the resonance frequencies was determined by fitting the spectra according to Eq. 1 and the corresponding results are summarized in Fig. 5.

All the modes show weak hardening towards lower temperatures followed by a tiny softening associated with the ferrimagnetic transition. Additionally, in  $\text{MnCr}_2\text{O}_4$  the first and second mode (located at  $\sim 195\text{ cm}^{-1}$  and  $\sim 376\text{ cm}^{-1}$ , respectively) are shifted toward higher energies upon the conical spin ordering at  $T_s=14\text{ K}$ . Although in  $\text{CoCr}_2\text{O}_4$  an anomalous broadening was observed for the third and fourth mode below  $T_C=93\text{ K}$ , no clear sign of phonon splitting can be discerned in either of the two compounds within the resolution of our experiment,  $\sim 0.5\text{ cm}^{-1}$ . These results are compatible with a very weak, if any, distortion of the cubic lattice in  $\text{MnCr}_2\text{O}_4$  and  $\text{CoCr}_2\text{O}_4$  even at T=10 K.

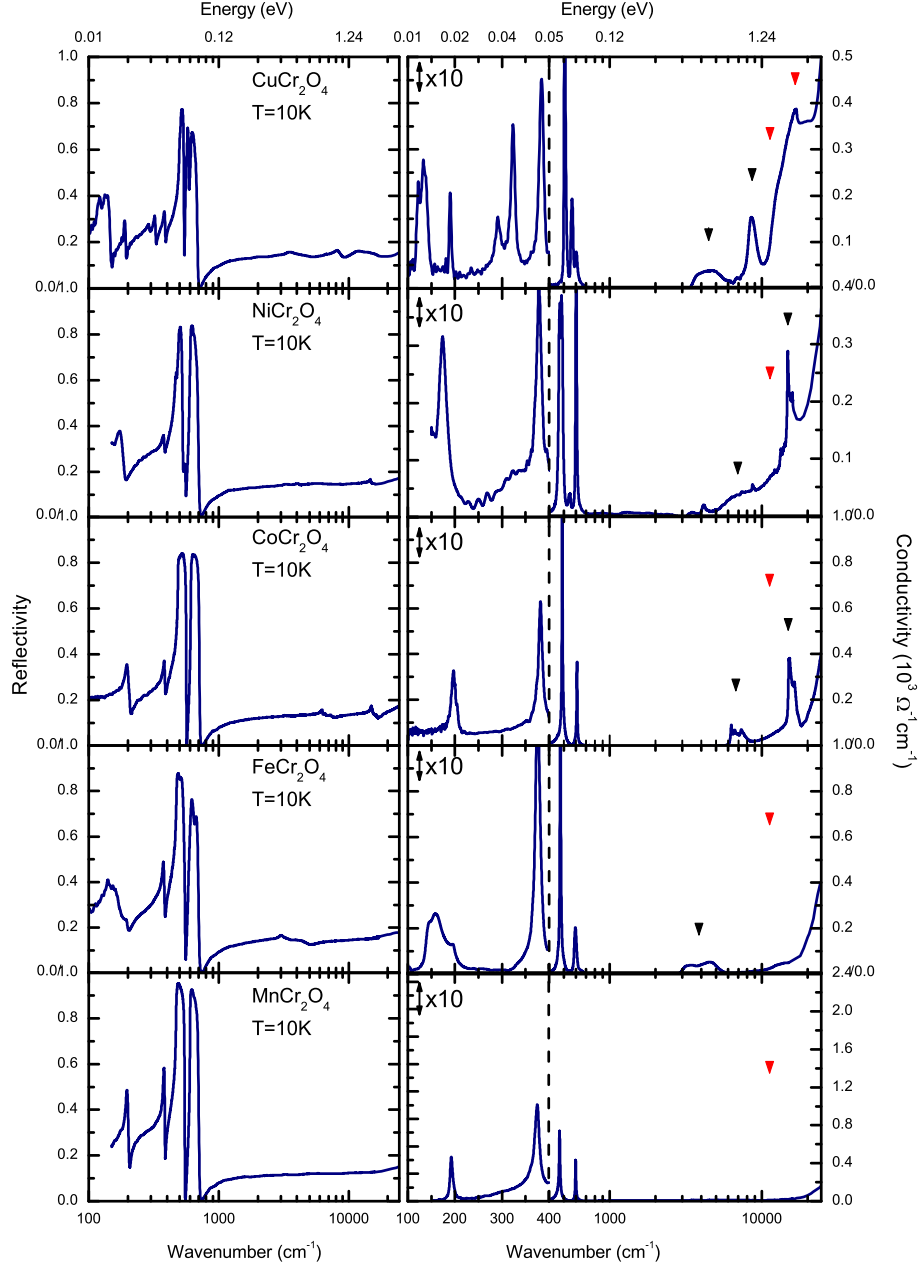


FIG. 2: Reflectivity spectra (left panel) and the real part of the optical conductivity spectra (right panel) over the photon energy range of  $100 \text{ cm}^{-1}$  and  $24\,500 \text{ cm}^{-1}$  for the  $\text{ACr}_2\text{O}_4$  ( $\text{A}=\text{Mn, Fe, Co, Ni and Cu}$ ) spinel crystals measured at  $T=10 \text{ K}$ . This spectral range covers the in-gap excitations, namely the optical phonon modes and the intraatomic 3d-3d transitions. The 3d-3d transitions of  $\text{A}^{2+}$  ions are indicated by black triangles, while the 3d-3d transitions of  $\text{Cr}^{3+}$  ions are shown with grey triangles. The low-energy part of the conductivity spectra is ten times magnified for better visibility. In  $\text{MnCr}_2\text{O}_4$  and  $\text{CoCr}_2\text{O}_4$  only the four  $T_{1u}(\text{IR})$  infrared active phonon modes corresponding to the cubic symmetry are visible. In the other compounds, some of these four modes are clearly split indicating the lowering of the crystal symmetry.

#### Phonon modes in $\text{ACr}_2\text{O}_4$ spinels with Jahn-Teller active ions

In  $\text{FeCr}_2\text{O}_4$  and  $\text{NiCr}_2\text{O}_4$  spinel oxides with Jahn-Teller active  $\text{A}^{2+}$  ions, the presence of four  $T_{1u}(\text{IR})$  phonon modes above room temperature, respectively fol-

lowed in Fig. 6 and Fig. 7, indicates the stability of the high-symmetry cubic spinel structure. However, upon the Jahn-Teller transition of  $\text{FeCr}_2\text{O}_4$  at  $T_{JT}=135 \text{ K}$  the lowest- and the highest-energy mode, while in  $\text{NiCr}_2\text{O}_4$  below  $T_{JT}=320 \text{ K}$  the two high-energy modes are split indicating structural transition to a tetragonal state.



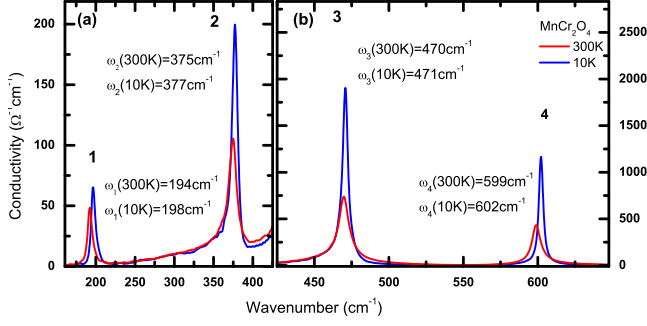


FIG. 3: Optical conductivity spectra of  $\text{MnCr}_2\text{O}_4$  at  $T=300$  K and 10 K contain four distinct phonon modes. Neither the ferrimagnetic transition at  $T_C=51$  K nor the onset of conical spin order at  $T_S=14$  K are accompanied with an observable splitting of these  $T_{1u}(\text{IR})$  phonon modes. Note that the conductivity scales for panel (a) and (b) differ by more than an order of magnitude.

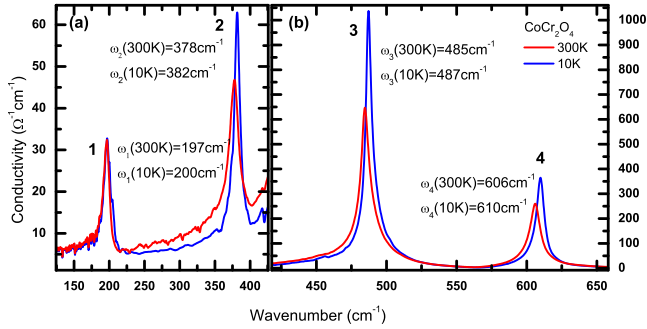


FIG. 4: Optical conductivity spectra of  $\text{CoCr}_2\text{O}_4$  at  $T=300$  K and 10 K. Similarly to  $\text{MnCr}_2\text{O}_4$ , no splitting of the four  $T_{1u}(\text{IR})$  phonon modes can be traced either below the ferrimagnetic transition at  $T_C=93$  K or upon the conical spin ordering at  $T_S=26$  K.

Besides the splitting of the third and fourth mode in  $\text{NiCr}_2\text{O}_4$ , a new excitation appears below the Jahn-Teller transition at  $\omega_5=545\text{ cm}^{-1}$  (see Fig. 7(c)). This fifth mode has low oscillator strength, short lifetime and cannot be deduced from either of the cubic  $T_{1u}(\text{IR})$  phonons. However, in the tetragonal phase the originally silent  $T_{2u}(\text{S})$  phonon mode can split into an infrared-active  $E_u(\text{IR})$  doublet and a silent  $B_{2u}(\text{S})$  singlet beside the splitting of the  $T_{1u}(\text{IR})$  modes to  $A_{2u}(\text{IR}) \oplus E_u(\text{IR})$ . We assign this weak mode around  $\omega_5=545\text{ cm}^{-1}$  to such an  $E_u(\text{IR})$  mode originating from one of the two  $T_{2u}(\text{S})$  modes silent in the cubic symmetry. Another mode with similarly small intensity emerges just below  $T_{JT}$  in the vicinity of the third  $T_{1u}(\text{IR})$  mode. We assign it as the other  $E_u(\text{IR})$  mode activated by the tetragonal splitting. The fact that the third  $T_{1u}(\text{IR})$  is split into two branches at  $T_{JT}$  and becomes three non-degenerate modes with comparable oscillator strength below  $T_C$  highly support

this assignment, i.e. it shows the independent origin of this weak mode.

The optical conductivity spectra of  $\text{CuCr}_2\text{O}_4$  are shown in Fig. 8. Each  $T_{1u}(\text{IR})$  mode is already split to  $A_{2u}(\text{IR}) \oplus E_u(\text{IR})$  at room temperature in accordance with its cubic to tetragonal phase transition at  $T_{JT}=854$  K. The remaining twofold degeneracy of each  $E_u(\text{IR})$  is lifted upon the ferrimagnetic transition. In contrast to  $\text{NiCr}_2\text{O}_4$ , no activation of silent modes can be followed.

A summary about the temperature dependence of the phonon frequencies are plotted in Fig. 9 for the spinel oxides with orbital degeneracy,  $A=\text{Fe, Ni and Cu}$ . The ferrimagnetic phase transition completely removes the threefold degeneracy of some of the cubic  $T_{1u}(\text{IR})$  modes in all the three compounds, therefore, the cubic symmetry of the lattice is lower than tetragonal in the ground state of these compounds. The modes whose degeneracy is partly lifted by the Jahn-Teller distortion exhibit further splitting at the subsequent magnetic transition at  $T_C$  except for the highest-energy mode in  $\text{NiCr}_2\text{O}_4$ . The magnetically induced splitting is as large as  $\Delta\omega/\omega \approx 10\%$  for the lower-energy vibrations. The sensitivity of the phonon modes to the magnetic ordering depends on the chemical composition; in  $\text{FeCr}_2\text{O}_4$  the first and the fourth modes, in  $\text{NiCr}_2\text{O}_4$  the third mode, while in  $\text{CuCr}_2\text{O}_4$  all modes are split. Furthermore, the ferroelectric phase transition in  $\text{FeCr}_2\text{O}_4$  is accompanied by a sudden hardening of the lower-energy modes. The partial activation of two silent  $T_{2u}(\text{S})$  vibrations was only observed in  $\text{NiCr}_2\text{O}_4$ . Among these new  $E_u(\text{IR})$  modes the vibration around  $\omega_5=545\text{ cm}^{-1}$  is sensitive to the magnetic ordering as it shows a splitting in the vicinity of  $T_C$ . As already reported in the literature [35], the lowest-energy mode in this compound exhibit an anomalous softening with decreasing temperature. Such unusual temperature dependence of the low-energy vibrations was also found in  $\text{FeV}_2\text{O}_4$  [35].

### Intra-3d-band excitations of A site ions

Weak in-gap excitations observed over the mid-infrared-visible range in  $\text{ACr}_2\text{O}_4$  spinels are interpreted as transitions within the  $3d$  levels of the A-site cations split by the local crystal field, the Coulomb interaction and the spin-orbit coupling [26]. In  $\text{ACr}_2\text{O}_4$  compounds these parity-forbidden transitions become allowed due to the lack of inversion symmetry in the local tetrahedral environment which provides the possibility to investigate the electronic structure of the A site ions by optical spectroscopy. In the subsequent section the optical conductivity spectra are analysed in terms of ligand field theoretical calculations.

We observed  $3d-3d$  excitations in the optical conductivity spectra of  $A=\text{Cu, Ni, Co}$  and  $A=\text{Fe}$  chromium

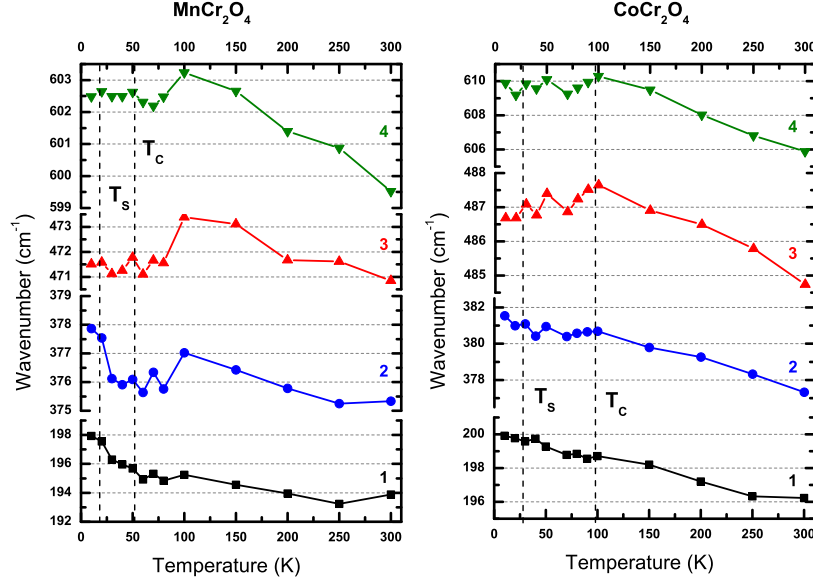


FIG. 5: Temperature dependence of phonon mode energies in  $\text{MnCr}_2\text{O}_4$  and  $\text{CoCr}_2\text{O}_4$ .  $\text{Mn}^{2+}$  and  $\text{Co}^{2+}$  ions, located on the A site of the spinel structure, have no orbital degeneracy (Fig. 1(b)). Correspondingly, no structural transition associated with a cooperative Jahn-Teller distortion has been observed. No measurable splitting of the phonon modes occur upon the magnetic phase transitions either.  $T_C$  and  $T_S$  label the transition to a ferrimagnetic state and to the ground state with conical spin order, respectively.

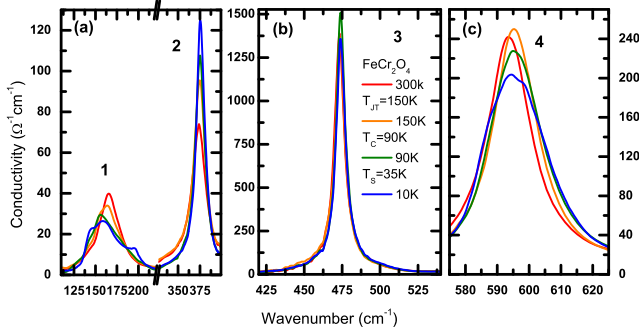


FIG. 6: Optical conductivity spectra of  $\text{FeCr}_2\text{O}_4$  at various temperatures in the vicinity of the Jahn-Teller transition at  $T_{JT}=135$  K, the ferrimagnetic ordering at  $T_C=93$  K and the onset of the conical order at  $T_S=35$  K. Lowering of the crystal symmetry can be traced as a temperature induced splitting of the lowest- and the highest-energy phonon modes both at  $T_{JT}$  and  $T_C$ , while splitting of the other two  $T_{1u}(\text{IR})$  modes cannot be resolved.

spinel oxides, while no such transition was found in  $\text{MnCr}_2\text{O}_4$  (see Fig. 2). The absence of this excitation in the latter compound indicates that high-spin state is realized for the A-site since there is no spin-allowed  $3d$ - $3d$  transition within the half-filled d-band of the  $\text{Mn}^{2+}$  ion in the presence of strong Hund-coupling as shown in Fig. 1(b).

Ohgushi et al. have discussed the case of A=Fe and Co in the frame of ligand field theory including spin-orbit

coupling [26]. The main results of their calculations are reproduced in the first two panel of Fig. 10. The transition in  $\text{FeCr}_2\text{O}_4$  at around  $\sim 0.49$  eV, was assigned as a single electron transition through the crystal field gap,  ${}^5\text{E}(\text{e}^3\text{t}_2^3) \rightarrow {}^5\text{T}_2(\text{e}^2\text{t}_2^4)$ , while the two absorption peaks in  $\text{CoCr}_2\text{O}_4$  at around  $\sim 0.84$  eV and  $\sim 1.95$  eV correspond to the  ${}^4\text{A}_2(\text{e}^4\text{t}_2^3) \rightarrow {}^4\text{T}_2(\text{e}^3\text{t}_2^4)$  and  ${}^4\text{A}_2(\text{e}^4\text{t}_2^3) \rightarrow {}^5\text{T}_1(\text{e}^3\text{t}_2^4)$  transitions, respectively. From these excitations the crystal field splitting corresponding to the cubic state and the Racah parameter, B, characteristic to the Coulomb interaction can be determined for  $\text{Co}^{2+}$ :  $\Delta\text{E}=0.84$  eV and  $\text{B}=0.083$  eV, respectively.

In the low-temperature optical conductivity spectrum of  $\text{NiCr}_2\text{O}_4$  two distinct structures are visible around  $\sim 0.95$  eV and  $\sim 1.94$  eV, which can be assigned as  $3d$ - $3d$  transitions of the tetrahedrally coordinated  $\text{Ni}^{2+}$ . Since the fine structure of these peaks cannot be resolved, cubic ( $T_d$ ) site symmetry was assumed in our model and the tetragonal distortion was neglected [36]. The energy levels of the eight 3d electron of the  $\text{Ni}^{2+}$ , relevant for the single particle excitations, is depicted in Fig. 10(c). The two peaks in the optical conductivity spectrum were fitted with two Lorentzian corresponding to the two electric-dipole-allowed transitions:  ${}^3\text{T}_1(\text{e}^4\text{t}_2^4) \rightarrow {}^3\text{T}_2(\text{e}^3\text{t}_2^5)$  and  ${}^3\text{T}_1(\text{e}^4\text{t}_2^4) \rightarrow {}^3\text{T}_1(\text{e}^3\text{t}_2^5)$  (see Fig. 11(a)). The cubic crystal field splitting and the Racah parameter for the  $\text{Ni}^{2+}$  ion were deduced from the transition energies:  $\Delta\text{E}=1.20$  eV and  $\text{B}=0.082$  eV, respectively. The spin-orbit and the unresolved tetragonal splitting may be

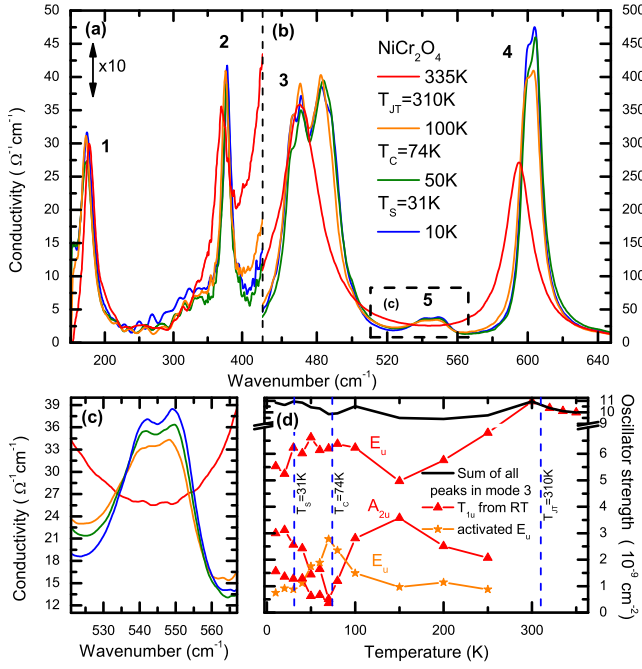


FIG. 7: (a-b) Optical conductivity spectra of  $\text{NiCr}_2\text{O}_4$  at various temperatures over the region of the Jahn-Teller transition at  $T_{JT} = 320$  K, the ferrimagnetic ordering at  $T_C = 74$  K and the onset of the canted magnetic structure at  $T_S = 31$  K. Splitting of the third and the fourth  $T_{1u}(\text{IR})$  modes can be observed both at  $T_{JT}$  and  $T_C$ . Scale of low energy part is magnified ten times larger. (c) Between these modes the activation of an  $E_u(\text{IR})$  mode, which originates from a  $T_{2u}(\text{S})$  mode being silent in the cubic phase, can be followed. Rigorous analysis shows the activation of another  $E_u(\text{IR})$  mode upon  $T_{JT}$ , which is located among the branches of the third  $T_{1u}(\text{IR})$  mode. (d) Oscillator strength for this  $E_u(\text{IR})$  mode and for the branches of the third  $T_{1u}(\text{IR})$  mode as a function of temperature.

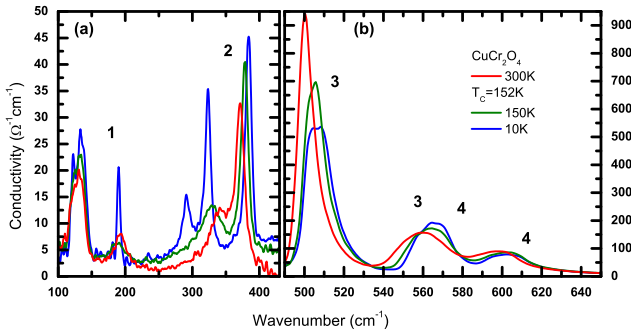


FIG. 8: Optical conductivity spectra of  $\text{CuCr}_2\text{O}_4$  at various temperatures. At room temperature all  $T_{1u}(\text{IR})$  phonon modes are split due to the Jahn-Teller transition at  $T_{JT} = 854$  K. For each mode the remaining degeneracy is lifted upon the magnetic ordering at  $T_C = 152$  K.

responsible for the large width of the resonances peaks.

In contrast to  $\text{NiCr}_2\text{O}_4$ , the crystal lattice of the

$\text{CuCr}_2\text{O}_4$  has strong tetragonal distortion at low temperature [17]. Perhaps, the low-symmetry of the lattice is responsible for the large number of peaks observed in the near infrared and visible part of the optical conductivity spectrum. As in other  $\text{ACr}_2\text{O}_4$  compounds the excitations around  $E = 1.6$  eV are assigned to the intra-atomic  $3d-3d$  transitions of  $\text{Cr}^{3+}$  split by the tetragonal distortion. Compared to the sister compounds the strength of this transition is remarkably enhanced. The two lower-energy peaks at around  $\sim 0.56$  eV and  $\sim 1.06$  eV are related to the  $3d-3d$  transitions of  $\text{Cu}^{2+}$ . Due to the strong Jahn-Teller distortion in the ligand field calculations tetragonal  $D_{2d}$  local symmetry was assumed and the spin-orbit coupling was also taken into account. The energy levels and the possible optical transitions are shown in Fig. 10(d). In the  $D_{2d}$  symmetry the  ${}^2B_2 \rightarrow {}^2B_1$  transition is forbidden, and only the spin-orbit interaction makes it weakly allowed, therefore, its oscillator strength was assumed to be zero. The optical conductivity spectrum was fitted with three Lorentzian oscillator as shown in Fig. 11(b). The obtained values for the cubic and the tetragonal crystal field splittings, and the spin-orbit coupling are  $\Delta E = 0.69$  eV,  $\Delta E_{t1} = 0.56$  eV and  $\zeta = 0.1$  eV, respectively, if the tetragonal splitting within the cubic  ${}^2E$  term,  $\Delta E_{t2}$  is neglected.

The different parameters of the electronic structure of the A-site ions, namely the cubic and tetragonal crystal field splittings,  $\Delta E$  and  $\Delta E_t$ , respectively, the Racah parameter,  $B$  and the strength of the spin-orbit coupling,  $\zeta$  are summarized in Table I for the investigated  $\text{ACr}_2\text{O}_4$  spinel oxides. These fundamental energy scales may serve as a starting point for a microscopic theory describing the magneto-elasticity of the  $\text{ACr}_2\text{O}_4$  spinels and provide in general an important input to theories describing their magnetic states.

TABLE I: Cubic ( $\Delta E$ ) and tetragonal ( $\Delta E_t$ ) crystal field splittings, the Racah parameter ( $B$ ) and the strength of the spin-orbit coupling ( $\zeta$ ) as determined in the present study for various spinel oxides with magnetic A-site ions.

	$\text{Fe}^{2+}$ [26]	$\text{Co}^{2+}$ [26]	$\text{Ni}^{2+}$	$\text{Cu}^{2+}$
$\Delta E$ (eV)	0.49	0.84	1.20	0.69
$\Delta E_{t1}, \Delta E_{t2}$ (eV)				0.56, $\sim 0$
$B$ (eV)		0.083	0.082	
$\zeta$ (eV)	0.13 ( ${}^5T_2$ )	0.25 ( ${}^4T_2$ ) 0.34 ( ${}^4T_1$ )		0.1 ( ${}^2T_2$ )

## Discussion

From the viewpoint of the dynamical properties of the lattice,  $\text{ACr}_2\text{O}_4$  chromium spinels ( $A = \text{Mn, Fe, Co, Ni}$

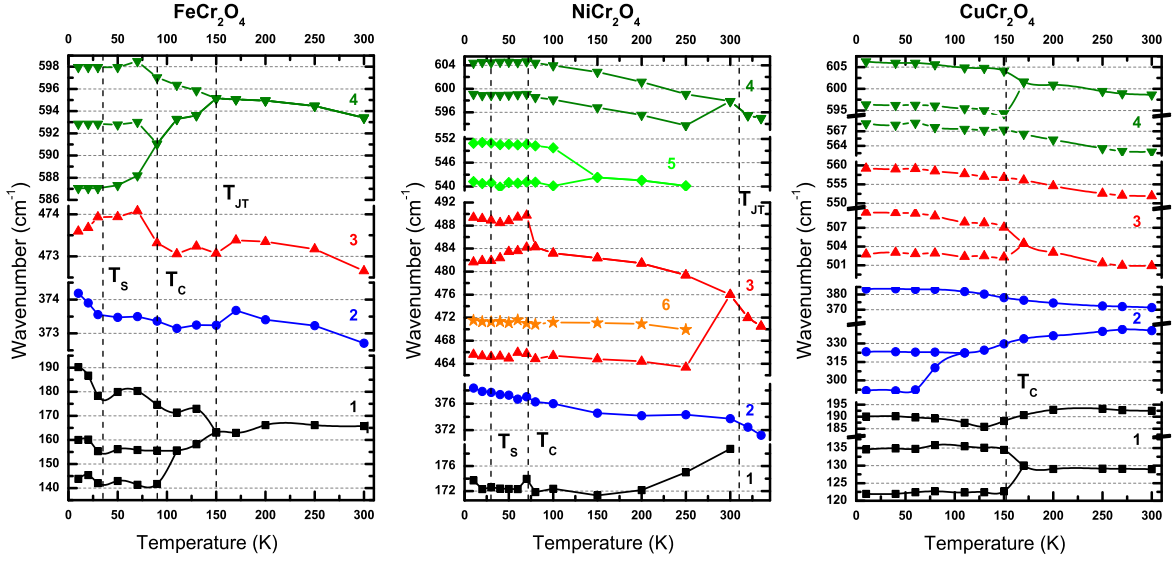


FIG. 9: Temperature dependence of phonon energies in  $\text{FeCr}_2\text{O}_4$ ,  $\text{NiCr}_2\text{O}_4$  and  $\text{CuCr}_2\text{O}_4$ . Lattice vibrations originating from the same  $T_{1u}$  and  $T_{2u}$  cubic modes are labeled with the same color and symbol. The temperature of the phase transitions are indicated by dashed lines.

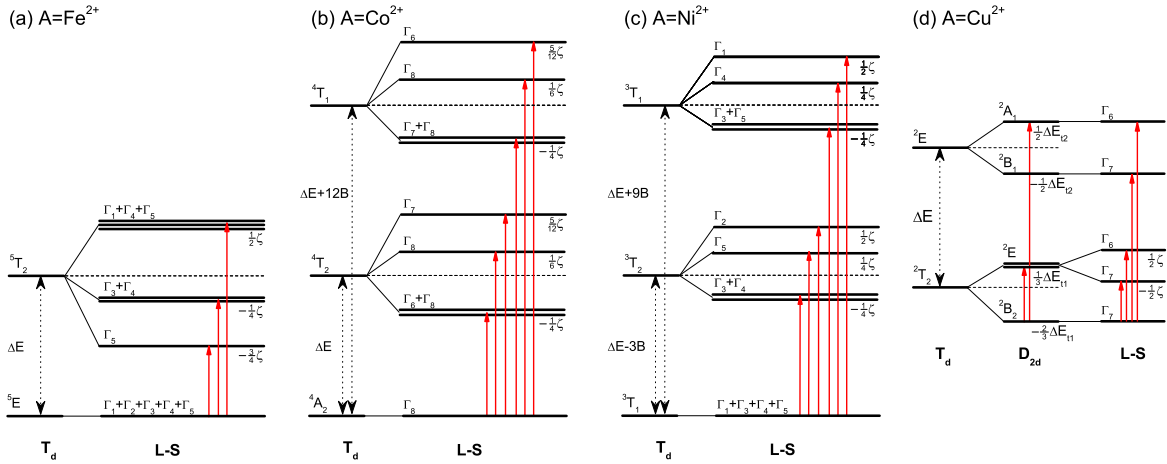


FIG. 10: Energy level diagrams corresponding to  $\text{Fe}^{2+}$ ,  $\text{Co}^{2+}$ ,  $\text{Ni}^{2+}$  and  $\text{Cu}^{2+}$  3d orbitals occupied by holes. In these diagrams only the spin-allowed single-particle excitations are shown, red arrows represents the allowed optical transitions. (a-b)  $3d-3d$  optical transitions within the d-band of the A-site ion split by the cubic ( $T_d$ ) crystal field,  $\Delta E$ , the Racah parameter,  $B$  and the spin-orbit interaction,  $\zeta$  for  $A=\text{Fe}^{2+}$  and  $A=\text{Co}^{2+}$  [26, 36]. (c) In case of  $A=\text{Ni}^{2+}$  the effect of local  $T_d$  symmetry and spin-orbit interaction was taken into account, the latter as the weakest perturbation. Here, symmetry lowering associated with the weak tetragonal splitting was neglected. (d) In case of  $A=\text{Cu}^{2+}$  the effect of Jahn-Teller distortion, i.e. tetragonal splitting,  $\Delta E_1$  was considered stronger than the spin-orbit interaction.

and Cu) can be classified into two distinct groups. The main results of our optical study about these classes are summarized in Fig. 5 and Fig. 9.

In the first group the A-site ions have no orbital degeneracy ( $A=\text{Mn}$  and  $\text{Co}$ ) and neither of these compounds show observable phonon mode splitting upon the magnetic phase transitions from room temperature down to  $T=10\text{ K}$ . Anomalous broadening of the third and fourth mode of  $\text{CoCr}_2\text{O}_4$  below  $T_C=93\text{ K}$  is observed,

which may indicate a mode splitting slightly below the spectral resolution of our experiment ( $\sim 0.5\text{ cm}^{-1}$ ). In  $\text{MnCr}_2\text{O}_4$  we could not even follow any broadening of the modes associated with the magnetic transitions. Therefore, we conclude that the magnetoelasticity is weak in these compounds and the cubic symmetry of the lattice is nearly preserved even in their magnetically ordered ground state.

For materials in the second class – where A-site ions



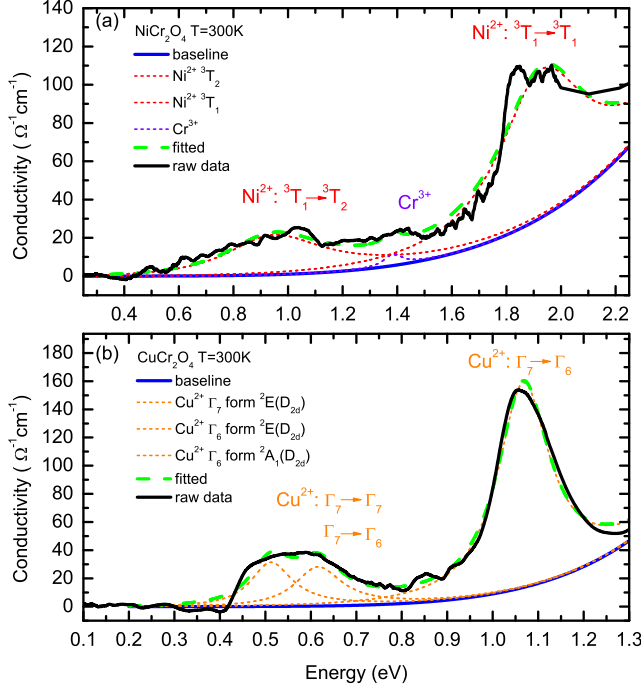


FIG. 11: Analysis of the intra-atomic  $3d-3d$  transitions in  $\text{NiCr}_2\text{O}_4$  and  $\text{CuCr}_2\text{O}_4$  as shown in panel (a) and (b), respectively. Labels correspond to notation introduced in Fig. 10. Besides the oscillators, there is a common baseline corresponding to the tail of the band edge.

are Jahn-Teller active, i.e. they have orbital degeneracy in the cubic phase – we observed phonon-mode splitting associated with the cooperative Jahn-Teller distortion. The sequence of the splittings shows that a cubic to tetragonal distortion takes place at  $T_{JT}$ . Phonon modes in  $\text{CuCr}_2\text{O}_4$  exhibit a relative splitting of  $\approx 30\%$ ,  $\approx 8\%$ ,  $\approx 9\%$  and  $\approx 7\%$  in ascending order of phonon energies already at room temperature [20]. For comparison, splitting of the third and fourth phonon modes in  $\text{NiCr}_2\text{O}_4$  is  $\approx 4\%$  and  $\approx 1\%$ , while the lowest- and highest-energy phonons in  $\text{FeCr}_2\text{O}_4$  are split by  $\Delta\omega/\omega_o \approx 20\%$  and  $\approx 1\%$ , respectively. Most of the modes whose degeneracy is partly lifted by the cooperative Jahn-Teller distortion or those activated upon the splitting of silent  $T_{2u}$  lattice vibrations, as is the case in  $\text{NiCr}_2\text{O}_4$ , are further split upon the ferrimagnetic ordering. The magnitude of the magnetically induced splitting is in the range of  $\approx 10\%$  for low-energy and  $\approx 1\%$  for high-energy phonon modes, the large splitting of low-energy modes implies strong spin-lattice coupling for these lattice vibrations resulting in the strong magnetoelastic effects. Recently, the static orthorhombic distortion of the crystalline lattice upon the magnetic phase transition has also been observed by means of high-resolution X-ray diffraction in  $\text{NiCr}_2\text{O}_4$  and  $\text{CuCr}_2\text{O}_4$  [37, 38].

In conclusions, we found that in  $\text{ACr}_2\text{O}_4$  spinel compounds – where the frustration of the pyrochlore sub-

lattice is lifted by long-range magnetic ordering due to the exchange interaction between the spins of the  $\text{A}^{2+}$  and  $\text{Cr}^{3+}$  ions – the criterion of strong magnetoelasticity is the orbital degeneracy of the A-site ion in the high-symmetry cubic phase. This observation is valid irrespective to the details of the magnetic order, i.e. we found strong magnetoelasticity for the compounds  $\text{FeCr}_2\text{O}_4$ ,  $\text{NiCr}_2\text{O}_4$  and  $\text{CuCr}_2\text{O}_4$  independently whether they have conical or canted spin order in their ground state. A theoretical model reproducing the effect of orbital occupancy on the magnetoelasticity of these compounds will be published elsewhere [39]. Moreover, based on the analysis of the intraatomic  $3d-3d$  transition of the A-site ions, we could determine the following fundamental energies: crystal-field splitting in the cubic and tetragonal phases, the Racah parameters representing the strength of the intraatomic Coulomb repulsion and the spin-orbit interaction in some cases.

### Acknowledgement

This work was supported by Hungarian Research Funds OTKA PD75615, Bolyai 00256/08/11, TÁMOP-4.2.2.B-10/1-2010-0009 and it was partly supported by Grant-in-Aid for Scientific Research (S) No. 24224009, and FIRST Program by the Japan Society for the Promotion of Science (JSPS). Financial support by the Deutsche Forschungsgemeinschaft through SFB 484 is acknowledged.

- 
- [1] J. Hemberger, P. Lunkenheimer, R. Fichtl, H.-A. Krug von Nidda, V. Tsurkan and A. Loidl, *Nature* **434**, 364 (2005).
  - [2] V. Gnezdilov, P. Lemmens, Yu. G. Pashkevich, Ch. Payen, K. Y. Choi, J. Hemberger, A. Loidl and V. Tsurkan, *Phys. Rev. B* **84**, 045106 (2011).
  - [3] A. B. Harris, T. Yildirim, A. Aharony and O. Entin-Wohlman, *Phys. Rev. B* **73**, 184433 (2006).
  - [4] Y. Takahashi, N. Kida, Y. Yamasaki, J. Fujioka, T. Arima, R. Shimano, S. Miyahara, M. Mochizuki, N. Furukawa and Y. Tokura, *Phys. Rev. Lett.* **101**, 187201 (2008).
  - [5] M. Mochizuki, N. Furukawa and N. Nagaosa, *Phys. Rev. Lett.* **105**, 037205 (2010).
  - [6] M. Mochizuki, N. Furukawa and N. Nagaosa, *Phys. Rev. B* **84**, 144409 (2011).
  - [7] Y. Yamasaki, S. Miyasaka, Y. Kaneko, J.-P. He, T. Arima and Y. Tokura, *Phys. Rev. Lett.* **96**, 207204 (2006).
  - [8] S. Weber, P. Lunkenheimer, R. Fichtl, J. Hemberger, V. Tsurkan and A. Loidl, *Phys. Rev. Lett.* **96**, 157202 (2006).
  - [9] N. Mufti, A. A. Nugroho, G. R. Blake and T. T. M. Palstra, *J. Phys. C* **22**, 075902 (2010).
  - [10] K. Singh, A. Maignan, C. Simon and C. Martin, *Appl. Phys. Lett.* **99**, 172903 (2011).

- [11] S. H. Lee, C. Broholm, T. H. Kim, W. Ratcliff and S. W. Cheong, Phys. Rev. Lett. **84**, 3718 (2000).
- [12] A. B. Sushkov, O. Tchernyshyov, W. Ratcliff, S.W. Cheong and H. D. Drew, Phys. Rev. Lett. **94**, 137202 (2005).
- [13] J. H. Chung, M. Matsuda, S.-H. Lee, K. Kakurai, H. Ueda, T. J. Sato, H. Takagi, K. P. Hong and S. Park, Phys. Rev. Lett. **95**, 247204 (2005).
- [14] T. Rudolf, Ch. Kant, F. Mayr, J. Hemberger, V. Tsurkan and A. Loidl, New J. Phys. **9**, 76 (2007).
- [15] E. Prince, J. Appl. Phys. **32**, 68S (1961).
- [16] M. Tanaka, T. Tokoro and Y. Aiyama, J. Phys. Soc. Japan **21**, 262 (1966).
- [17] O. Crottaz, F. Kubel and H. Schmid, J. Matter. Chem. **7**, 143 (1997).
- [18] B. J. Kennedy and Q. Zhou, J. Solid State Chem. **181**, 2227 (2008).
- [19] J. M. Hastings and L. M. Corliss, Phys. Rev. **126**, 2 (1962).
- [20] S. Bordács, D. Varjas, I. Kézsmárki, G. Mihály, L. Baldassarre, A. Abouelsayed, C. A. Kuntscher, K. Ohgushi and Y. Tokura, Phys. Rev. Lett. **103**, 077205 (2009).
- [21] T. Katsufuji, T. Suzuki, H. Takei, M. Shingu, K. Kato, K. Osaka, M. Takata, H. Sagayama and T. Arima, J. Phy. Soc. Jpn. **77**, 053708 (2008).
- [22] T. A. Kaplan and N. Menyuk, Philos. Mag. **87**, 3711 (2007).
- [23] N. Menyuk, K. Dwight and A. World, J. Phys. (Paris) **25**, 528 (1964).
- [24] S. Funahasi, Y. Midorii and H.R. Child, J. Appl. Phys. **61**, 4114 (1987).
- [25] K. Tomiyasu, J. Fukunaga and H. Suzuki, Phys. Rev. B **70**, 214434 (2004).
- [26] K. Ohgushi, Y. Okimoto, T. Ogasawara, S. Miyasaka and Y. Tokura, J. Phy. Soc. Jpn. **77**, 034713 (2008).
- [27] G. Shirane, D. E. Cox, and S. J. Pickart, J. Appl. Phys. **35**, 954 (1964).
- [28] G. L. Bacchella and M. Pinot, J. Phys. (Paris) **25**, 537 (1964).
- [29] S. Klemme, H. S. C. O'Neill, W. Schnelle, and E. Gmelin, Am. Miner. **85**, 1686 (2000).
- [30] H. Ishibashi and T. Yasumi, J. Magn. Magn. Mat. **310**, e610 (2007).
- [31] K. Tomiyasu and I. Kagomiya, J. Phys. Soc. Japan **73**, 2539 (2004).
- [32] E. Prince, Acta Cryst. **10**, 554 (1957).
- [33] B. M. Wanklyn, F. R. Wondre and W. Davison, J. Mat. Sci. **11**, 1607 (1976).
- [34] High energy spectra of  $\text{MnCr}_2\text{O}_4$  was used to extend the reflectivity of  $\text{NiCr}_2\text{O}_4$  above 3eV.
- [35] K. Siratori, J. Phys. Soc. Japan **23**, 948 (1967).
- [36] S. Sugano, Y. Tanabe and H. Kamimura: *Multiplets of transition metal ions in crystals*, 1970 Academic Press, New York and London.
- [37] H. Ishibashi and T. Yasumi, J. Mag. Mag. Mat. **310**, 610 (2006).
- [38] M. R. Suchomel, D. P. Shoemaker, L. Ribaud, M. C. Kemei and Ram Seshadri, Phys. Rev. B **86**, 054406 (2012).
- [39] V. Kocsis et al., unpublished results